Macromolecules

pubs.acs.org/Macromolecules Article

Deformation Driven Deswelling of Brush Gels

Michael Jacobs, Yuan Tian, and Andrey V. Dobrynin*

Cite This: Macromolecules 2023, 56, 2209−2216 Read Online

ACCESS | Metrics & More | Article Recommendations | Supporting Information

ABSTRACT: We studied equilibrium swelling in brush gels undergoing large uniaxial deformations in contact with solvent by using a combination of the Flory−Rehner and scaling models of gels and coarse-grained molecular dynamics simulations of swollen brush networks. Our analysis showed that the swelling ratio of the brush gels $Q_{eq}(\lambda)$, describing the volume change upon swelling, is a nonmonotonic function of the gel uniaxial deformation ratio λ characterizing the gel shape. It first increases with increasing strand elongation from its value for the free-standing gel then begins to decrease. This behavior is a result of the optimization of polymer/solvent interactions and conformational entropy of brush strands in the nonlinear deformation regime. The location of the maximum in the $Q_{eq}(\lambda)$ function is directly related to the value of the strain-stiffening parameter β. This parameter depends on the degree of polymerization of the brush backbone and the backbone Kuhn length defined by both the grafting density and degree of polymerization of the side chains. Analysis of the nonlinear gel modulus confirmed that the strain-stiffening parameter β is identical in both dry networks and gels. However, the structural modulus of the gels, G_s, is smaller than that of the dry networks, G_{dr}, by a factor equal to the ratio of the Kuhn length of brush strands in the dry state, b_K, and in the gel, $b_{K,s}$, such that $G_s = G_{dr}b_K/b_{K,s}$.

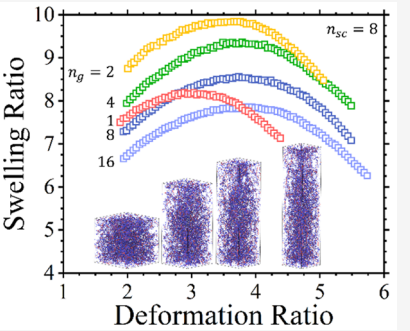

INTRODUCTION

Polymer gels are mechanochemical systems capable of absorbing solvent, the amount of which is defined by the environmental conditions.[1−6] In their pioneering paper over 70 years ago, Katchalsky et al.[7−9] envisioned gels to become a synthetic analogue of human muscles which could controllably actuate by responding to variation of solution pH. Since then, gels have intertwined various aspects of life as absorbing materials broadly used in agriculture and consumer goods, drug delivery systems, implantable devices, 3D manufacturing, and water purification systems.[10−21] Recent advances in polymer chemistry culminating in the synthesis of brush-like polymers[22−24] (Figure 1) have solved a long-standing problem of polymer networks and gels associated with constraints imposed on their mechanical properties by entanglements.[25−31] This opened a new direction in network design with a focus on strand architecture[27,28,30,32,33] producing mechanically diverse gels of brush networks with similar solvent content[34] analogous to living tissues and with their volumes V demonstrating up to 50 times[34−36] increase from the dry state value, V_0.

The large volumetric changes of brush gels result in nonlinear strand deformations unusual for gels of linear chains.[5,6] In order to account for this effect, the classical Flory−Rehner[1,2,37] and scaling[5] models of gel swelling were modified by incorporating finite strand extensibility.[35,38] The improved gel models explained the observed correlations between the gel modulus and the swelling ratio $Q = V/V_0$ of the free-standing gels and pinpointed the origin of gel mechanical diversity.[38] Building on this success, we derive a general expression for the mechanochemical response of brush gels undergoing large uniaxial deformations in contact with surrounding solvent. This allows gels to adjust the solvent content with deformation by optimizing their shape. The freedom in solvent exchange with surroundings is manifested

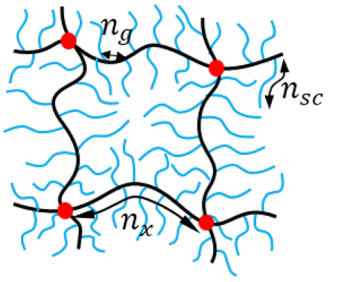

Figure 1. Network of brush strands with the number of the backbones between cross-links n_x, side-chain degree of polymerization n_{sc}, and grafting density $1/n_g$ (n_g is the number of backbone bonds between grafted side chains). The partitioning of monomers between backbones and side chains is characterized by the composition $\varphi = n_g/(n_g + n_{sc})$. Backbones are shown by black lines and side chains are colored in blue.

Received: November 23, 2022
Revised: February 6, 2023
Published: February 22, 2023

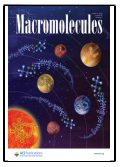

https://doi.org/10.1021/acs.macromol.2c02385
Macromolecules 2023, 56, 2209−2216

in a nonmonotonic dependence of the gel swelling ratio Q on deformation such that at large deformations the gel expels solvent, reaching a solvent content below the level of free-standing gels. This peculiar behavior is confirmed by new molecular dynamics simulations of the uniaxial deformation of brush gels covering both linear and nonlinear deformation regimes.

The rest of the paper is organized as follows. We begin with a derivation of the expressions governing network mechano-chemical response by using the Flory–Rehner[1,2,37] and scaling[5] approaches. This is followed by testing of the model predictions in molecular dynamics simulations of nonlinear deformation of swollen brush networks at a constant pressure transversal to the deformation direction, mimicking the conditions of the solvent exchange in implicit solvent simulations.

SWELLING AND DEFORMATION OF GELS

Consider a network (Figure 1) made of brush-like strands with the number of backbone bonds between cross-links n_x, side-chain degree of polymerization n_{sc}, and grafting density $1/n_g$ (n_g is the number of backbone bonds between grafted side chains) which has initial dimensions $L_{0,i}$ ($i = x, y$, and z) and initial volume $V_0 = L_{0,x}L_{0,y}L_{0,z}$ in the dry state (Figure 2). The

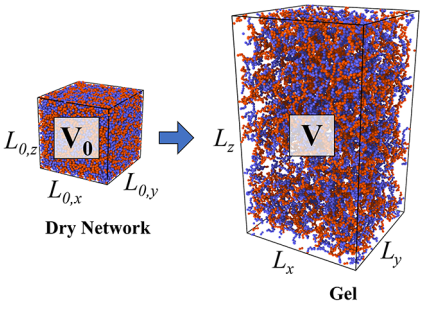

Figure 2. Swelling and deformation of dry brush network from volume V_0 to volume V. Brush backbones are shown in red, and side chains are colored in blue.

network swells and undergoes deformation reaching dimensions L_i and volume $V = L_xL_yL_z$. The final state of the gel is characterized by the elongation $\lambda_i = L_i/L_{0,i}$ and swelling $Q = V/V_0$ ratios quantifying shape and volumetric changes with respect to the dry state. The total Helmholtz free energy of the swollen and deformed network surrounded by a solvent is a sum

$$F_{total} = F_{elast}(\{L_i\}) + F_{gel}(V, \rho_g, \rho_{sol,g}) + F_{sol}(V_{sol}, \rho_{sol}) \quad (1)$$

of the elastic free energy of the gel, $F_{elast}(\{L_i\})$, the free energy of the gel/solvent system, $F_{gel}(V, \rho_g, \rho_{sol,g})$ describing solvent distribution in the gel and interactions of monomers and solvent with densities ρ_g and $\rho_{sol,g}$, respectively, and free energy of the solvent, $F_{sol}(V_{sol}, \rho_{sol})$, occupying the volume V_{sol} outside the gel at a solvent density ρ_{sol}. We assume that the total volume of the gel/solvent system, V_{total}, does not change upon network swelling and deformation such that $V_{total} = V + V_{sol} =$ constant. Below we will use different models accounting for the gel's elastic and interaction terms in eq 1 to describe the gel's mechanochemical equilibrium upon large uniaxial deformations.

Flory–Rehner Model. In the framework of the Flory–Rehner approach,[1,2,37] the elastic response of the network strands does not change with swelling such that the elastic free energy of a gel with semiflexible strands in the entire deformation range can be written as follows:[35,38,39]

$$F_{elast}^{FR}(\{L_i\}) = \frac{1}{6}V_0G_{dr}I_1(1 + 2(1 - \beta I_1/3)^{-1}) \quad (2)$$

where $I_1 = \lambda_x^2 + \lambda_y^2 + \lambda_z^2$ is the first deformation invariant expressed in terms of the deformation ratios λ_i. There are two parameters in eq 2 that relate the network's deformation and swelling ability to its structure: (i) the strain-stiffening parameter (strand elongation ratio) β and (ii) the structural shear modulus in the dry state, G_{dr}. The parameter $\beta = \langle R_{in}^2\rangle/R_{max}^2$ is a ratio of the mean-square end-to-end distance of a network strand between cross-links $\langle R_{in}^2\rangle$ in the undeformed network and the square of the end-to-end distance of a fully extended strand, $R_{max}^2 = n_x^2l^2$, with monomer projection length l and degree of polymerization of network strands between cross-links n_x. The structural modulus of a dry network with monomer number density ρ_0 made by cross-linking brush strands with the Kuhn length b_K is equal to[35,38,40]

$$G_{dr} = Ck_BT\frac{\rho_0\varphi}{n_x}\frac{\langle R_{in}^2\rangle}{b_KR_{max}} \quad (3)$$

where C is a numerical constant that accounts for the network topology and cross-link functionality, k_B is the Boltzmann constant, T is the absolute temperature, and $\varphi = n_g/(n_g + n_{sc})$ is the brush composition which describes the partitioning of monomers between the side chains and the backbone (see Figure 1). Note that in addition to the brush composition the brush strand structure is included through the Kuhn length's dependence on n_g and n_{sc}.[38,41]

The true stress generated in the deformed gel under uniaxial elongation along the z-axis is equal to

$$\sigma_{zz} = \frac{1}{L_xL_y}\frac{\partial F_{total}}{\partial L_z} = \frac{V_0}{L_xL_y}\frac{L_z}{L_{0,z}^2}\frac{G_{dr}}{3}(1 + 2(1 - \beta I_1/3)^{-2}) + \frac{\partial F_{gel}(V, \rho_g, \rho_{sol,g})}{\partial V} - \frac{\partial F_{sol}(V_{sol}, \rho_{sol})}{\partial V_{sol}} \quad (4)$$

In the directions x and y, no external force is applied such that

$$0 = \frac{1}{L_xL_z}\frac{\partial F_{total}}{\partial L_y} = \frac{V_0}{L_xL_z}\frac{L_y}{L_{0,y}^2}\frac{G_{dr}}{3}(1 + 2(1 - \beta I_1/3)^{-2}) + \frac{\partial F_{gel}(V, \rho_g, \rho_{s,g})}{\partial V} - \frac{\partial F_{sol}(V_{sol}, \rho_s)}{\partial V_{sol}} \quad (5)$$

A similar expression can be written down for the x component. It is convenient to rewrite eqs 4 and 5 in terms of the deformation ratios λ_i, swelling ratio of the gel Q, and gel osmotic pressure

$$\pi(Q) = -\partial F_{gel}/\partial V + \partial F_{sol}/\partial V_{sol} \quad (6)$$

as follows:

$$\sigma_{zz} = \frac{G_{dr}}{3}\frac{\lambda_z}{\lambda_x\lambda_y}(1 + 2(1 - \beta I_1/3)^{-2}) - \pi(Q) \quad (7a)$$

https://doi.org/10.1021/acs.macromol.2c02385
Macromolecules 2023, 56, 2209−2216

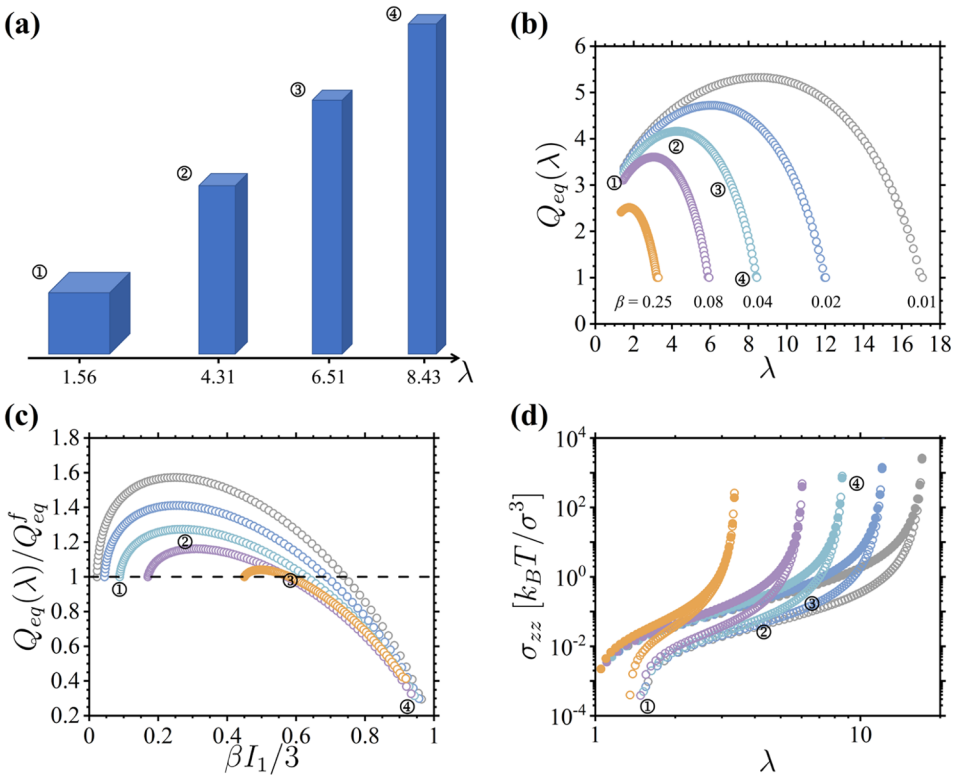

Figure 3. (a) Schematic representation of gel shape as a function of deformation ratio λ. (b) Dependence of equilibrium swelling ratio $Q_{eq}(\lambda)$ on the deformation ratio λ calculated by numerically solving eqs 9a and 9b with osmotic pressure given by eq 10 and monomer excluded volume v = 1.25 σ^3 (σ is monomer diameter) for networks with dry shear modulus G_{dr} = 0.01 k_BT/σ^3 and different values of strand elongation ratios β = 0.01 (gray circles), 0.02 (blue circles), 0.04 (cyan circles), 0.08 (purple circles), and 0.25 (orange circles). (c) Dependence of $Q_{eq}(\lambda)/Q^f_{eq}$ on $\beta I_1(Q, \lambda)/3$ for gels shown in panel b. (d) True stress in uniaxially deformed gels shown in panels b and c and corresponding dry networks. Open symbols represent gels, and filled symbols show dry networks.

$$0 = \frac{G_{dr}}{3}\frac{\lambda_y}{\lambda_z\lambda_x}(1 + 2(1 - \beta I_1/3)^{-2}) - \pi(Q) \tag{7b}$$

For uniaxial gel deformation, the combination of gel swelling and deformation is characterized by two independent variables λ and Q quantifying the change of the gel shape and occupied volume such that

$$\lambda_z = \lambda;\ \ Q = \lambda_x\lambda_y\lambda_z;\ \ \lambda_x = \lambda_y = \sqrt{Q/\lambda};\ \ I_1 = \lambda^2 + 2Q/\lambda \tag{8}$$

In terms of these variables, eqs 7a and 7b can be transformed into

$$\sigma_{zz} = \frac{G_{dr}}{3}\left(\frac{\lambda^2}{Q} - \frac{1}{\lambda}\right)(1 + 2(1 - \beta I_1/3)^{-2}) \tag{9a}$$

$$\frac{G_{dr}}{3\lambda}(1 + 2(1 - \beta I_1/3)^{-2}) = \pi(Q) \tag{9b}$$

For the free-standing gels, σ_{zz} = 0, resulting in $\lambda = Q^{1/3} = \lambda_x = \lambda_y$ (eq 8), and eq 9b reduces to the classical Flory–Rehner expression defining equilibrium gel swelling ratio, Q^f_{eq}, by balancing network shear modulus and osmotic pressure.

To highlight the effect of gel deformation on equilibrium swelling, we assume that the solvent is a θ-solvent with monomer excluded volume v

$$\pi(Q) = \frac{k_BT}{v}\frac{Q^{-3}}{3} \tag{10}$$

Figures 3a–d summarize the results of the numerical solution of eqs 9a and 9b with osmotic pressure term given by eq 10. Figure 3a shows gel shape variations starting from equilibrium swelling state described by Q^f_{eq} to highly asymmetric deformation. The evolution of the gel swelling ratio $Q_{eq}(\lambda)$ with deformation ratio λ is illustrated in Figure 3b. It follows from this figure that with increasing gel deformation, the swelling ratio $Q_{eq}(\lambda)$ first increases and then starts to decrease. The decrease in $Q_{eq}(\lambda)$ indicates that gels shrink upon deformation to minimize strand elongation caused by a combination of stretching and swelling. The location of the maximum monotonically shifts to the left (smaller λ) with increasing value of the strain stiffening parameter β directly correlating with strand deformation in a free-standing gel (Figure 3b). The effect of nonlinear strand deformation is more convenient to see by normalizing $Q_{eq}(\lambda)$ of the uniaxially deformed gels by its value for free-standing gels Q^f_{eq} and plot it as a function of $\beta I_1/3$ (Figure 3c). This selection of the variables for the x-axis corresponds to representing swelling/deformation data as a function of the ratio $\langle R^2(\lambda)\rangle/R_{max}^2$, which characterizes the degree of elongation of the network strands with respect to their fully extended state. Thus, deformation induced deswelling occurs at gel stress corresponding to the nonlinear strand deformation regime (Figure 3d). This is consistent with decrease in the height of the maximum (Figures 3b,c) with increasing β since it requires less stretching of the preswollen short strands to reach the nonlinear deformation regime. For comparison, Figure 3d

https://doi.org/10.1021/acs.macromol.2c02385
Macromolecules 2023, 56, 2209–2216

also shows the stress evolution in dry networks. The deformation curves for gels and dry networks converge when extension of the network strands approaches the fully extended chain limit. At such deformations, a significant amount of solvent is expelled from the network (see Figures 3b,c) reducing gel behavior to that of the dry network.

It is important to point out that eqs 9a and 9b can be adapted to describe the stress and volume change in the dry network undergoing uniaxial deformation by substituting atmospheric pressure P_{atm} instead of the solvent pressure and using the Flory–Huggins equation of state[1,2] with the free volume and without the strands "ideal gas" term, $k_BT\rho_0/n_x$, to describe pressure in a network. This will account for a change of the dry network volume under uniaxial deformation. For small deformations, eq 9b expresses the network Poisson ratio in terms of the shear and bulk moduli. Note, however, that the volume changes in dry networks upon deformations are not as dramatic as in gels since a solvent could be viewed as a free volume on steroids as explained in the Supporting Information.

Scaling Model. The approach developed above can be extended to correctly account for changes in the strands' elastic response in a good solvent or in the case of brush-like strands for which the effective Kuhn length is different in the dry and gel states due to significantly stronger steric repulsion between swollen side chains.[38] Following the formalism developed in ref 38, we model a brush gel as a semidilute polymer solution[5,42]

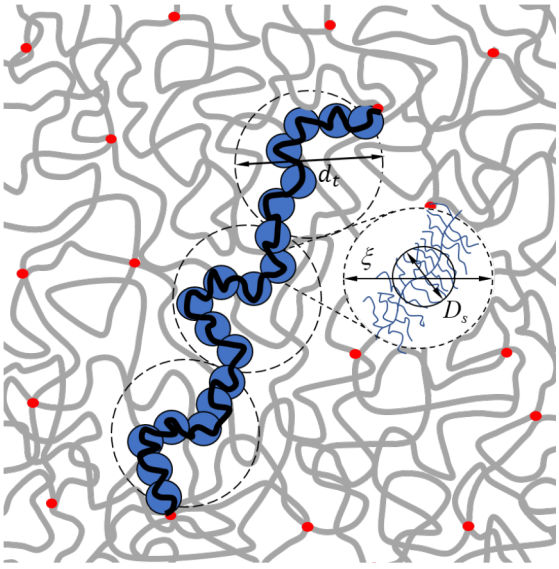

Figure 4. Schematic representation of hierarchical blob structure of brush strands in a gel as a semidilute solution of stretched filaments with tension blob size d_t, correlation length ξ, and filament thickness D_s which determines the Kuhn length and excluded volume of the brush strand. Adapted with permission from ref 38.

of stretched filaments with correlation length ξ (Figure 4) which elastic energy is given by the following expression:

$$F_{elast}^{Scaling}(\{L_i\}) \approx \frac{1}{6}V_0G_{dr}\frac{b_K l g_\xi}{\xi^2}I_1(1 + 2(1 - \beta I_1/3)^{-1}) \tag{11}$$

The factor of ξ^2/lg_ξ can be viewed as the Kuhn length of the chain of correlation blobs each containing g_ξ backbone monomers in the case of the brush-like strands. In a semidilute solution, the correlation length ξ contains sections of brushes with g_ξ backbone monomers[43,44]

$$\xi = l g_\xi^{\ \nu}/B \tag{12}$$

where exponent ν = 0.588 and 0.5 for good and θ solvents, respectively. The parameter B characterizes the interactions between a polymer and a solvent, assuming values B_g and B_{th} in good and θ solvents. In the general case, it can be written in terms of the excluded volume v_s per monomer of the backbone and the Kuhn length, $b_{K,s}$, of the network strand in a solvent as follows:[43,44]

$$B = \left(\frac{l}{b_{K,s}}\right)^{0.5}\left(\frac{v_s}{(l b_{K,s})^{1.5}}\right)^{1-2\nu} \tag{13}$$

Using relationships between the number of backbone monomers per correlation blob, g_ξ, and correlation length, ξ[38]

$$g_\xi \approx B^{3/(3\nu-1)}\left(\frac{Q}{\varphi\rho_0 l^3}\right)^{1/(3\nu-1)} \tag{14.a}$$

$$\xi \approx lB^{1/(3\nu-1)}\left(\frac{Q}{\varphi\rho_0 l^3}\right)^{\nu/(3\nu-1)} \tag{14.b}$$

we can express the ratio

$$\frac{lg_\xi}{\xi^2} \approx l^{-1}B^{1/(3\nu-1)}\left(\frac{Q}{\varphi\rho_0 l^3}\right)^{(1-2\nu)/(3\nu-1)} \tag{15}$$

in terms of the swelling ratio and polymer specific parameters. Thus, this correction introduces an additional dependence of the gel shear modulus on its volume through the factor Q. The Q correction disappears in a θ solvent where exponent ν = 0.5 and $B = B_{th}$, which only accounts for changes in the Kuhn length of the solvated strands $B_{th} = (l/b_{K,s})^{0.5}$.

Substituting the scaling expression for the gel elastic energy eq 11 into eqs 4 and 5, we arrive at

$$\sigma_{zz} = \frac{G_s}{3}\left(\frac{\lambda^2}{Q} - \frac{1}{\lambda}\right)(1 + 2(1 - \beta I_1/3)^{-2}) \tag{16a}$$

$$\frac{G_s}{3\lambda}(1 + 2(1 - \beta I_1/3)^{-2}) - \frac{(2\nu - 1)}{(3\nu - 1)}\frac{F_{elast}^{Scaling}(\{L_i\})}{V_0Q} \approx \frac{k_BT}{\xi^3} \tag{16b}$$

where the structural gel modulus, G_s, in the framework of the scaling model is equal to

$$G_s = G_{dr}\frac{b_K}{l}B^{1/(3\nu-1)}\left(\frac{Q}{\varphi\rho_0 l^3}\right)^{(1-2\nu)/(3\nu-1)} \tag{17}$$

It follows from eqs 16a and 16b that in addition to the explicit dependence of the gel structural modulus on the swelling ratio (eq 17) there is a new term promoting gel swelling which depends on the elasticity of the swollen network strands (eq 16b). In the next section we will illustrate how these new features, incorporated into the scaling model of gel deformation and swelling, influence a combination of deformation and swelling of brush gels.

https://doi.org/10.1021/acs.macromol.2c02385
Macromolecules 2023, 56, 2209−2216

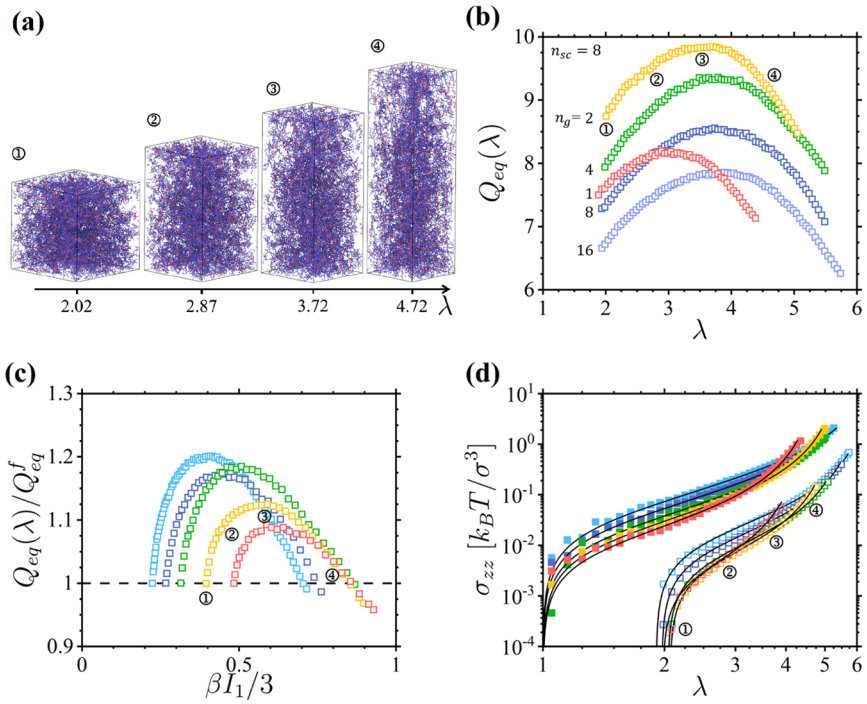

Figure 5. (a) Snapshots illustrating the evolution of the shape of the simulation box with deformation ratio λ. (b) Dependence of the equilibrium swelling ratio $Q_{eq}(\lambda)$ on deformation ratio λ for brush networks with n_x = 16, n_{sc} = 8, and different values of side-chain grafting densities characterized by n_g = 1 (red symbols), n_g = 2 (yellow symbols), n_g = 4 (green symbols), n_g = 8 (blue symbols), and n_g = 16 (light blue symbols). (c) Dependence of $Q_{eq}(\lambda)/Q^f_{eq}$ on $\beta I_1(Q,\lambda)/3$ for gels shown in panel b. (d) True stress in uniaxially deformed gels shown in panel b and for the same networks in a dry (melt) state. Open symbols correspond to gels and filled symbols represent data for dry networks. Solid lines are the best fit to eq 16 with fitting parameters G_s, G_d, and β summarized in Table S1.

COMPARISON WITH SIMULATIONS

We performed coarse-grained molecular dynamics simulations of the deformation of swollen brush networks (gels) undergoing uniaxial deformations at fixed pressure transversal to the deformation direction. The networks of brush strand interacting through pure repulsive Lennard-Jones potential were prepared in a dry state with initial monomer density $0.8\sigma^{-3}$ by cross-linking ends of the side chains of precursor brush macromolecules having backbone degree of polymerization n_{bb} = 129 as described in our previous publications[35,38] and summarized in the Supporting Information. In this new set of simulations, the swollen networks were deformed by incrementally increasing the dimensions of the simulation box along the z-direction maintaining pressure in the x and y directions constant at P = 0.0 corresponding to the equilibrium pressure of free-standing gels. The constant pressure was achieved by using Nosé−Hoover barostat in the x and y directions implemented in LAMMPS.[45] This effectively allowed the volume of the simulation box to change upon gel deformation mimicking a solvent migration in and out of the swollen network. The simulation details are summarized in the Supporting Information together with all data sets.

Figure 5a shows the shape evolution of a gel upon deformation. This is quantified in Figures 5b,c for the swelling ratio $Q_{eq}(\lambda)$ for gels with comb and bottlebrush strands. As in the case of analytically calculated gel swelling curves (Figures 3b,c), we observe a nonmonotonic dependence of the swelling ratio (Figure 5b) and normalized swelling ratio (Figure 5c) with network deformation. At sufficiently large deformation, the gels start to release solvent which is manifested in a decrease of the swelling ratio $Q_{eq}(\lambda)$ below its equilibrium value in the free-standing gel, Q^f_{eq}. For comparison with theoretically calculated stress−elongation curves (Figure 3d), similar curves for gels are shown in Figure 5d. The main difference between simulation and theoretical curves is that in simulations the bonds of the deformed network strands can stretch. This bond deformation slows down the convergence of the deformation curves obtained for swollen and dry networks, eliminating divergence of the network stress as network strands approach the fully extended limit (Figure 5d). Note that at large deformations ($\beta I_1/3 > 0.7$) the observed trend in the decrease of $Q_{eq}(\lambda)/Q^f_{eq}$ with gel deformation corresponds to a crossover to the bond stretching regime and a change of the brush effective Kuhn length as side chains belonging to neighboring strands start to overlap. Furthermore, for brush gels with densely grafted side chains, n_g = 1, the location of the maximum is already at the onset of the bond stretching due to strong strand deformation at equilibrium swelling of the free-standing gel.

Figure 6 establishes correlations between Q_{max} and brush composition φ, describing partitioning of the monomers between backbones and side chains. The maximum swelling ratio Q_{max} increases with increasing both the distance between grafting points of the side chains n_g and their degree of polymerization n_{sc}. This is not surprising because increasing n_g weakens the prestretching of the brush backbone while an increase in n_{sc} promotes strand swelling ability. A similar plot for Q_{max} vs φ is shown in the Supporting Information.

Analysis of the fitting results, shown by the solid lines in Figure 5d, indicates that the values of the β parameters are identical in both swollen and dry networks, confirming the validity of the functional form of eq 11. The values of the

https://doi.org/10.1021/acs.macromol.2c02385
Macromolecules 2023, 56, 2209−2216

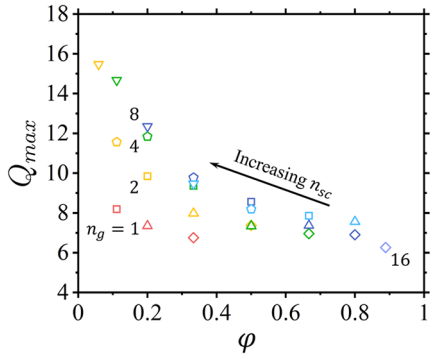

Figure 6. Dependence of Q_{max} on brush strand composition φ for gels with n_x = 16, different values of n_{sc} and n_g = 1 (red symbols), n_g = 2 (yellow symbols), n_g = 4 (green symbols), n_g = 8 (blue symbols), and n_g = 16 (light blue symbols).

structural modulus G_s in the swollen state are consistently smaller than corresponding values in the dry state G_{dr}, which is in agreement with eq 17. For brush gels the exponent ν = 0.5 due to a stiffening of the brush strands caused by the steric repulsion between swollen side chains[38] such that

$$G_s = G_{dr} b_K / b_{K,s} \tag{18}$$

Thus, the ratio of the moduli G_s/G_{dr} is proportional to the ratio of the corresponding Kuhn lengths in the dry and swollen states, resulting in $G_s < G_{dr}$ due to the swelling-induced stiffening of the brush strands. The difference between G_s and G_{dr} also indicates a breakdown of the Flory−Rehner approach which was already pointed out in ref 38.

To highlight the universality of the nonlinear network deformation in both dry and swollen states, Figure 7 shows the

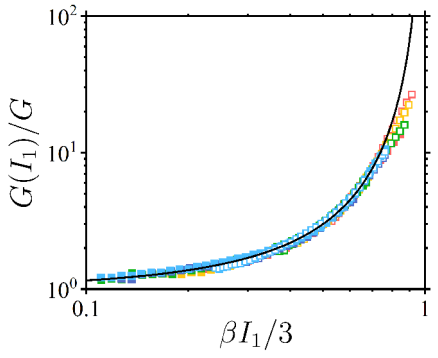

Figure 7. Dependence of the normalized deformation dependent modulus $G(I_1)/G$ on $\beta I_1/3$ for dry networks (filled symbols) and gels (open symbols) made of strands with n_x = 16 and n_{sc} = 8 and different values of n_g = 1 (red symbols), n_g = 2 (yellow symbols), n_g = 4 (green symbols), n_g = 8 (blue symbols), and n_g = 16 (light blue symbols). The solid line is given by eq 19.

dependence of the normalized deformation-dependent modulus

$$G(I_1) \equiv \frac{\sigma_{zz}}{\lambda^2/Q - \lambda^{-1}} = \frac{G}{3}\left(1 + 2\left(1 - \frac{\beta I_1}{3}\right)^{-2}\right) \tag{19}$$

where the structural modulus G is equal to G_{dr} for dry networks (Q = 1) and to G_s for gels with Q > 1. The deviation from the universal curve takes place at onset of the bond stretching and side-chain overlap in shrinking gels.

CONCLUSION

We study mechanochemical equilibrium in brush gels using a combination of analytical calculations based on the Flory−Rehner and scaling models and molecular dynamics simulations. It is shown that stretching a gel in contact with a solvent results in a nonmonotonic dependence of the swelling ratio on deformation (Figures 3b,c and 5b,c). The location of the maximum gel swelling is a function of the strand molecular architecture shifting to larger λ values with decreasing brush grafting density and degree of polymerization of the side chains (Figure 6). At sufficiently large deformations, we observe gel deswelling which is driven by minimization of the strands' elastic energy at the expense of polymer/solvent affinity. The functional form of the deformation-dependent modulus defining the nonlinear mechanical response is identical in both dry and swollen networks (eq 19). The specifics of the network strand architecture appear in the renormalization of the structural modulus (eq 18) due to steric repulsion between swollen side chains manifested in effective backbone stiffening (Figure 7). This renormalization of the structural gel modulus is the main reason behind the breakdown of the Flory−Rehner approach in brush gel elasticity. However, despite this, the Flory−Rehner model with a nonlinear elastic term correctly captures the qualitative features of gel deswelling at large deformations (see sets in Figures 3 and 5).

The analysis of the nonlinear deformation of gels presented here can be extended to describe the swelling and deformation of polyelectrolyte gels[9,46−51] at low and moderate salt concentrations for which nonlinear strand deformation effects are significant. The developed framework can be adapted to account for confinement and swelling of gels in a capillary.[52] In this case, a gel confinement induces elongation along the capillary similar to uniaxial gel deformation with an additional constraint imposed by the capillary walls. Furthermore, the demonstrated strong effect of gel deformation on swelling ratio could be important for the design of gel-based implantable devices in which solvent exchange with surrounding tissue could be extremely important for implant longevity. In such systems, the established coupling between gel deformation and swelling in open systems could result in solvent leaking into a tissue from implants upon deformation. We hope that the presented results will initiate research in this direction.

ASSOCIATED CONTENT

Supporting Information

The Supporting Information is available free of charge at https://pubs.acs.org/doi/10.1021/acs.macromol.2c02385.

Analytical calculation of Q_{max}, Poisson ratio of dry networks and volume change upon deformation, simulation details, and data sets (PDF)

AUTHOR INFORMATION

Corresponding Author

Andrey V. Dobrynin − *Department of Chemistry, University of North Carolina, Chapel Hill, North Carolina 27599-3290, United States;* orcid.org/0000-0002-6484-7409; Email: avd@email.unc.edu

Authors

Michael Jacobs − *Department of Chemistry, University of North Carolina, Chapel Hill, North Carolina 27599-3290, United States; Center for Nanophase Materials Sciences, Oak*

https://doi.org/10.1021/acs.macromol.2c02385
Macromolecules 2023, 56, 2209−2216

Ridge National Laboratory, Oak Ridge, Tennessee 37830, United States; orcid.org/0000-0002-7255-3451

Yuan Tian − *Department of Chemistry, University of North Carolina, Chapel Hill, North Carolina 27599-3290, United States;* orcid.org/0000-0002-7277-1408

Complete contact information is available at: https://pubs.acs.org/10.1021/acs.macromol.2c02385

Notes

The authors declare no competing financial interest.

■ ACKNOWLEDGMENTS

This work was supported by the National Science Foundation under Grant DMR 2049518.

■ REFERENCES

(1) Flory, P. J. *Principles of Polymer Chemistry*; Cornell University Press: Ithaca, NY, 1971.
(2) Treloar, L. R. G. *The Physics of Rubber Elasticity*; Clarendon Press: Oxford, 1975.
(3) McKenna, G. B. Soft matter: rubber and networks. *Rep. Prog. Phys.* **2018**, *81*, No. 066602.
(4) Peppas, N. A.; Hilt, J. Z.; Khademhosseini, A.; Langer, R. Hydrogels in biology and medicine: from molecular principles to bionanotechnology. *Adv. Mater.* **2006**, *18*, 1345−1360.
(5) Rubinstein, M.; Colby, R. H. *Polymer Physics*; Oxford University Press: New York, 2003.
(6) Horkay, F.; McKenna, G. B. Polymer Networks and Gels. In *Physical Properties of Polymers Handbook*; Mark, J. E., Ed.; Springer: New York, 2007; pp 497−523.
(7) Kuhn, W.; Hargitay, B.; Katchalsky, A.; Eisenberg, H. Reversible dilation and contraction by changing the state of ionization of high-polymer acid networks. *Nature* **1950**, *165*, 514−517.
(8) Katchalsky, A.; Eisenberg, H. Polyvinylphosphate contractile systems. *Nature* **1950**, *166*, 267−268.
(9) Katchalsky, A. Solutions of polyelectrolytes and mechanochemical systems. *J. Polym. Sci.* **1951**, *7*, 393−412.
(10) Wichterle, O.; Lim, D. Hydrophilic gels for biological use. *Nature* **1960**, *185*, 117−118.
(11) Buchholz, F. L.; Graham, A. T. *Modern Superabsorbent Polymer Technology*; Wiley-VCH: New York, 1998.
(12) Brannon-Peppas, L.; Harland, R. S. Absorbent polymer technology. *J. Controlled Release* **1991**, *17*, 297−298.
(13) Roy, D.; Cambre, J. N.; Sumerlin, B. S. Future perspectives and recent advances in stimuli-responsive materials. *Prog. Polym. Sci.* **2010**, *35*, 278−301.
(14) Hoffman, A. S. Hydrogels for biomedical applications. *Adv. Drug Delivery Rev.* **2002**, *54*, 3−12.
(15) Guilherme, M. R.; Aouada, F. A.; Fajardo, A. R.; Martins, A. F.; Paulino, A. T.; Davi, M. F. T.; Rubira, A. F.; Muniz, E. C. Superabsorbent hydrogels based on polysaccharides for application in agriculture as soil conditioner and nutrient carrier: A review. *Eur. Polym. J.* **2015**, *72*, 365−385.
(16) Zhang, Y.; Chan, H. F.; Leong, K. W. Advanced materials and processing for drug delivery: the past and the future. *Adv. Drug Delivery Rev.* **2013**, *65*, 104−120.
(17) Shaviv, A. Advances in controlled-release fertilizers. *Adv. Agronomy* **2001**, *71*, 1−49.
(18) Zhang, Y. S.; Khademhosseini, A. Advances in engineering hydrogels. *Science* **2017**, *356*, eaaf3627.
(19) Guo, Y.; Bae, J.; Fang, Z.; Li, P.; Zhao, F.; Yu, G. Hydrogels and Hydrogel-Derived Materials for Energy and Water Sustainability. *Chem. Rev.* **2020**, *120*, 7642−7707.
(20) Ligon, S. C.; Liska, R.; Stampfl, J. r.; Gurr, M.; Mülhaupt, R. Polymers for 3D Printing and Customized Additive Manufacturing. *Chem. Rev.* **2017**, *117*, 10212−10290.
(21) Kazanskii, K. S.; Dubrovskii, S. A. Chemistry and physics of agricultural hydrogels. *Adv. Polym. Sci.* **1992**, *104*, 97−133.
(22) Sumerlin, B. S.; Neugebauer, D.; Matyjaszewski, K. Initiation efficiency in the synthesis of molecular brushes by grafting from via atom transfer radical polymerization. *Macromolecules* **2005**, *38*, 702−708.
(23) Sheiko, S. S.; Sumerlin, B. S.; Matyjaszewski, K. Cylindrical Molecular Brushes: Synthesis, Characterization, and Properties. *Prog. Polym. Sci.* **2008**, *33*, 759−785.
(24) Matyjaszewski, K. Atom Transfer Radical Polymerization (ATRP): Current Status and Future Perspectives. *Macromolecules* **2012**, *45*, 4015−4039.
(25) Daniel, W. F. M.; Burdynska, J.; Vatankhah-Varnoosfaderani, M.; Matyjaszewski, K.; Paturej, J.; Rubinstein, M.; Dobrynin, A. V.; Sheiko, S. S. Solvent-free, supersoft and superelastic bottlebrush melts and networks. *Nat. Mater.* **2016**, *15*, 183−189.
(26) Liang, H.; Morgan, B. J.; Xie, G.; Martinez, M. R.; Zhulina, E. B.; Matyjaszewski, K.; Sheiko, S. S.; Dobrynin, A. V. Universality of the Entanglement Plateau Modulus of Comb and Bottlebrush Polymer Melts. *Macromolecules* **2018**, *51*, 10028−10039.
(27) Vatankhah-Varnosfaderani, M.; Daniel, W. F. M.; Everhart, M. H.; Pandya, A. A.; Liang, H. Y.; Matyjaszewski, K.; Dobrynin, A. V.; Sheiko, S. S. Mimicking biological stress-strain behaviour with synthetic elastomers. *Nature* **2017**, *549*, 497−501.
(28) Vatankhah-Varnosfaderani, M.; Keith, A. N.; Cong, Y. D.; Liang, H. Y.; Rosenthal, M.; Sztucki, M.; Clair, C.; Magonov, S.; Ivanov, D. A.; Dobrynin, A. V.; Sheiko, S. S. Chameleon-like elastomers with molecularly encoded strain-adaptive stiffening and coloration. *Science* **2018**, *359*, 1509−1513.
(29) Dalsin, S. J.; Hillmyer, M. A.; Bates, F. S. Linear Rheology of Polyolefin-Based Bottlebrush Polymers. *Macromolecules* **2015**, *48*, 4680−4691.
(30) Pakula, T.; Zhang, Y.; Matyjaszewski, K.; Lee, H. I.; Boerner, H.; Qin, S. H.; Berry, G. C. Molecular Brushes as Super-Soft Elastomers. *Polymer* **2006**, *47*, 7198−7206.
(31) Hu, M.; Xia, Y.; McKenna, G. B.; Kornfield, J. A.; Grubbs, R. H. Linear Rheological Response of a Series of Densely Branched Brush Polymers. *Macromolecules* **2011**, *44*, 6935−6943.
(32) Sheiko, S. S.; Everhart, M. H.; Dobrynin, A. V.; Vatankhah-Varnosfaderani, M. Encoding tissue mechanics in silicone. *Science Robotics* **2018**, *3*, eaat7175.
(33) Sheiko, S. S.; Dobrynin, A. V. Architectural code for rubber elasticity: From supersoft to superfirm materials. *Macromolecules* **2019**, *52*, 7531−7546.
(34) Sheiko, S. S.; Vashahi, F.; Morgan, B. J.; Maw, M.; Dashtimoghadam, E.; Fahimipour, F.; Jacobs, M.; Keith, A. N.; Vatankhah-Varnosfaderani, M.; Dobrynin, A. V. Mechanically Diverse Gels with Equal Solvent Content. *ACS Cent. Sci.* **2022**, *8*, 845−852.
(35) Jacobs, M.; Liang, H.; Dashtimoghadam, E.; Morgan, B. J.; Sheiko, S. S.; Dobrynin, A. V. Nonlinear Elasticity and Swelling of Comb and Bottlebrush Networks. *Macromolecules* **2019**, *52*, 5095−5101.
(36) Sarapas, J. M.; Chan, E. P.; Rettner, E. M.; Beers, K. L. Compressing and Swelling To Study the Structure of Extremely Soft Bottlebrush Networks Prepared by ROMP. *Macromolecules* **2018**, *51*, 2359−2366.
(37) Flory, P. J.; Rehner, J. Statistical mechanics of cross-linked polymer networks II. Swelling. *J. Chem. Phys.* **1943**, *11*, 521−526.
(38) Jacobs, M.; Vashahi, F.; Maw, M.; Sheiko, S. S.; Dobrynin, A. V. Brush gels: Where theory, simulations and experiments meet. *Macromolecules* **2022**, *55*, 7922−7931.
(39) Dobrynin, A. V.; Carrillo, J.-M. Y. Universality in nonlinear elasticity of biological and polymeric networks and gels. *Macromolecules* **2011**, *44*, 140−146.
(40) Liang, H.; Sheiko, S. S.; Dobrynin, A. V. Supersoft and Hyperelastic Polymer Networks with Brushlike Strands. *Macromolecules* **2018**, *51*, 638−645.

(41) Liang, H.; Wang, Z.; Sheiko, S. S.; Dobrynin, A. V. Comb and bottlebrush graft copolymers in a melt. *Macromolecules* **2019**, *52*, 3942−3950.
(42) De Gennes, P.-G. *Scaling Concepts in Polymer Physics*; Cornell University Press: Ithaca, NY, 1979.
(43) Dobrynin, A. V.; Jacobs, M. When Do Polyelectrolytes Entangle? *Macromolecules* **2021**, *54*, 1859−1869.
(44) Dobrynin, A. V.; Jacobs, M.; Sayko, R. Scaling of Polymer Solutions as a Quantitative Tool. *Macromolecules* **2021**, *54*, 2288−2295.
(45) Thompson, A. P.; Aktulga, H. M.; Berger, R.; Bolintineanu, D. S.; Brown, W. M.; Crozier, P. S.; in 't Veld, P. J.; Kohlmeyer, A.; Moore, S. G.; Nguyen, T. D.; Shan, R.; Stevens, M. J.; Tranchida, J.; Trott, C.; Plimpton, S. J. LAMMPS - a flexible simulation tool for particle-based materials modeling at the atomic, meso, and continuum scales. *Comput. Phys. Commun.* **2022**, *271*, 108171.
(46) Dobrynin, A. V. Theory and simulations of charged polymers: From solution properties to polymeric nanomaterials. *Curr. Opin. Colloid Interface Sci.* **2008**, *13*, 376−388.
(47) Dobrynin, A. V. Polyelectrolyte Solutions and Gels. In *Oxford Handbook of Soft Matter*; Terentjev, E., Weitz, D., Eds.; Oxford University Press: Oxford, 2014; pp 269−344.
(48) Harland, R.; Prud'homme, R. *Polyelectrolyte Gels*; American Chemical Society: Washington, DC, 1992.
(49) Khokhlov, A. R.; Starodubtzev, S. G.; Vasilevskaya, V. V. Conformational Transitions in Polymer Gels - Theory and Experiment. *Adv. Polym. Sci.* **1993**, *109*, 123−175.
(50) Kosovan, P.; Richter, T.; Holm, C. Modeling polyelectrolyte gels in equilibrium with salt solutions. *Macromolecules* **2015**, *48*, 7698−7708.
(51) Rubinstein, M.; Colby, R. H.; Dobrynin, A. V.; Joanny, J. F. Elastic modulus and equilibrium swelling of polyelectrolyte gels. *Macromolecules* **1996**, *29*, 398−406.
(52) Li, Y.; Sariyer, O. S.; Ramachandran, A.; Panyukov, S.; Rubinstein, M.; Kumacheva, E. Universal behavior of hydrogels confined to narrow capillaries. *Sci. Rep.* **2015**, *5*, 17017.

https://doi.org/10.1021/acs.macromol.2c02385
Macromolecules 2023, 56, 2209−2216